The Impact of Aircraft Data on an Atlantic Cyclone Analyzed in Terms of Sensitivities and Trajectories

BÉATRICE POUPONNEAU, FRANCK AYRAULT, THIERRY BERGOT, AND ALAIN JOLY

Météo-France, Centre National de Recherches Météorologiques, Toulouse, France

(Manuscript received 20 October 1997, in final form 14 October 1998)

ABSTRACT

A case study of an eastern Atlantic cyclogenesis event is conducted. The focus is on the impact of aircraft data on both the analysis and forecast of the event. The case takes place between 1 and 3 February 1994 and involves a phase of explosive deepening.

Several new techniques are brought to bear on this problem. An automatic tracking algorithm of vorticity maxima allows the construction of the cyclogenesis scenario in a relatively objective way. It also provides a clear depiction of some of the problems met in a sample of test forecasts. The origin of these problems is determined by employing the adjoint technique in order to point out which parts of the initial conditions are important in explaining the divergences between forecasts.

The cyclogenesis is shown to result from successive baroclinic interactions of a surface vorticity maxima with two upper-level structures in a finite-length baroclinic zone. The largest impact on the forecast is shown to result not from a direct influence of the upper-level observations, but rather from an indirect effect via the observation selection algorithm. While the cyclone development clearly involves upper-level–low-level interaction, the most detrimental difference in initial conditions originates at low levels.

1. Introduction

One of the challenging issues of the Fronts and Atlantic Storm-Track Experiment (FASTEX) (Joly et al. 1997) is that the predictability of land-falling wave cyclones is currently limited because they are initiated in data-sparse areas in the middle of oceanic storm tracks. The specification of initial conditions over cyclone breeding areas are expected to be one of the keys to forecast improvement. A potentially invaluable source for identifying and tracing jet streaks or other upper-level anomalies and precursors over these areas is available: commercial aircraft data. In this study, the impact of commercial aircraft data on dynamical structures such as potential vorticity (PV) anomalies (Hoskins et al. 1985) is evaluated. The impact of this data on the development of an Atlantic cyclone (from 1 to 3 February 1994) is investigated. The following three questions are addressed: (i) How are the changes brought to the analysis by aircraft data translated into forecast differences; (ii) can these changes be interpreted in the light of conceptual models of cyclogenesis; (iii) how are differences between analyses related to changes of the observing system.

Corresponding author address: Dr. Alain Joly, Météo-France, CNRM/GMME, 42, avenue G. Coriolis, F-31057 Toulouse Cedex, France.
E-mail: alain.joly@meteo.fr

The use of aircraft observations in operational numerical weather prediction has started with the manual AIREP message. Winds and temperature observations at flight level are vocally sent every 10° longitude. More recently, two kinds of onboard installations allow for automatic transmission of meteorological observations: the Aircraft to Satellite Data Relay (ASDAR system) and the Aeronautical Radio Incorporated (ARINC) Communication Addressing and Reporting System (ACARS). AIREP and ASDAR are mostly used over oceans (Atlantic and Pacific), while ACARS is used over continental areas (United States, Europe, and Australia). Thanks to the automatic nature of the system, the quality of the data has been improved (Brewster et al. 1989): ACARS winds are more accurate by design than rawinsonde upper-level winds [see Lenshow (1986) for a detailed discussion of errors from aircraft observations].

The studies of the impact of aircraft data and the observing system conducted in recent years show two features: (i) the use of AIREP and U.S. ACARS statistically improves the large-scale, short- and medium-range forecasts [there has been improvement of the rms error scores by up to 4%; Bell et al. (1994)], especially the upper-level forecast winds over the oceans (Kelly et al. 1993). Their effect is highly visible downstream of radiosonde data-sparse areas, as well as on the vertical structures analyzed through assimilation cycles. Because of the significant increase of both the quantity and

quality of aircraft data since the study of Kelly et al. (1993), one can assume that the impact of actual aircraft data would be greater than the one documented in their paper. (ii) The significant benefit from the inclusion of aircraft data is confirmed when its impact is evaluated at the synoptic scale. A good space–time distribution of aircraft data over synoptic structures important to the subsequent development is enough to improve forecasts (Graham 1994; Lorenc et al. 1988).

Perturbations in the initial conditions due to the assimilation of aircraft data may be complicated. Within the set of all the possible analysis changes, finding those modifications that improve the forecast may become difficult. However, a new way to address this problem has been proposed by Talagrand and Courtier (1987): if a forecast aspect representing the phenomenon of interest is selected, a diagnostic function J, the perturbations in the initial conditions that are most likely to create significant changes to the forecast measured by J can be quantified. This is done by integrating the adjoint model transposed in time.[1] Applying such an approach, one can define the aspect of the initial conditions to which a given meteorological phenomenon is most sensitive. Rabier et al. (1992) sucessfully apply this approach to an idealized baroclinic instability case. A review of the use of adjoint models as tools for sensitivity analysis, and their limitations, is given in Errico (1997).

Because the present work is part of the FASTEX program, the present case has been selected among cases of ''type B'' baroclinic development [using the terminology of Petterssen and Smebye (1971)]. Previous studies were based on a failure of the forecast: which is not the case for the current study. The focus is on the forecasted accuracy rather than occurrence of the event. The errors located with the adjoint are set within a dynamical context combining a subjective approach supplemented by a diagnostic of cyclone trajectories: the automatic tracking algorithm developed by Ayrault (1995). It will be shown that this kind of objective technique greatly helps the conceptualization of cyclogenesis scenario.

A series of analysis and forecasts of the cyclone life cycle are presented in section 2. In section 3, the dynamics of the cyclogenesis is detailed based on the reference experiment, and part of the forecast error is shown to be related to a mishandling of the life cycle as revealed by the tracking algorithm. In section 4, the adjoint technique is used to complete the understanding of the error in the 60-h forecasts. Summary and conclusions are given in section 5.

[1] Each time step of a model integration can be represented by a matrix and the time integration process is a matrix product. The adjoint is the transpose of this process, its time integration is therefore the product, in reverse order, of the transpose of each time step matrix. The sign of the time step is not changed.

2. Series of analysis and forecasts of the cyclone life cycle

The case chosen for this study was a strong cyclone that was well forecast by the French operational numerical weather prediction modeling system (ARPEGE). Other impact studies on single cases usually look into severe storms or less well forecasted cases (Heming 1990; Graham 1994; Lorenc et al. 1988).

a. The main features of the case study

On 31 January 1994, an undulating zonal front off the east coast of the United States was moving slowly eastward. A number of weak lows started to appear and one of them developed into the cyclone of interest. A low pressure center (later called A) initially developed along this front near 35°N, 72°W, with the most intense 850-hPa vorticity increase between 1200 UTC 31 January and 1800 UTC 1 February. At 1200 UTC 1 February (Fig. 1), a second center of low pressure (1005 hPa, called B) formed near 39°N, 55°W and started to amplify. Its maximum deepening phase took place between 0000 UTC 2 February and 0000 UTC 3 February with a rate of 36 hPa in 24 h (from 998 hPa in the vicinity of 42°N, 40°W to 962 hPa near 49°N, 16°W; Fig. 2, shown as a bold line) as it crossed the intense zonal jet stream. The cyclone reached the southwest of Ireland at 1200 UTC 3 February with an analyzed central pressure of 957 hPa (954 hPa observed). It continued its northward track while filling, on 4 February. At 300 hPa, the circulation was characterized by a zonal jet stream intensifying from 80 to 95 m s^{-1}. Further details on the evolution of the cyclone will be given in section 3.

Behind the cold front, convective development was observed, with strong winds, rainshowers, and hail at times. At 1200 UTC 3 February, mean wind speeds of 40 and 50 kt were observed over the Brittany and northeast Ireland coasts, respectively. Also, intense snowfall and rainfall were observed over the United Kingdom (Fig. 3).

b. Data assimilation system

Experiments are performed with the operational data assimilation and forecasting model (ARPEGE/IFS) at Météo-France (Courtier et al. 1991). Since 1987, Météo-France and the European Centre for Medium-Range Weather Forecasts (ECMWF) have developed this new forecast system. One of the main goals of this project was to develop a global spectral model on a stretched grid (Courtier and Geleyn 1988). The assimilation scheme chosen for the version of ARPEGE, in the present study, is a classic 3D multivariate optimal interpolation scheme: CANARI. Intermittent analyses on the model grid, at model levels and for model historical variables, are carried out with a 6-h cycle. To deal with

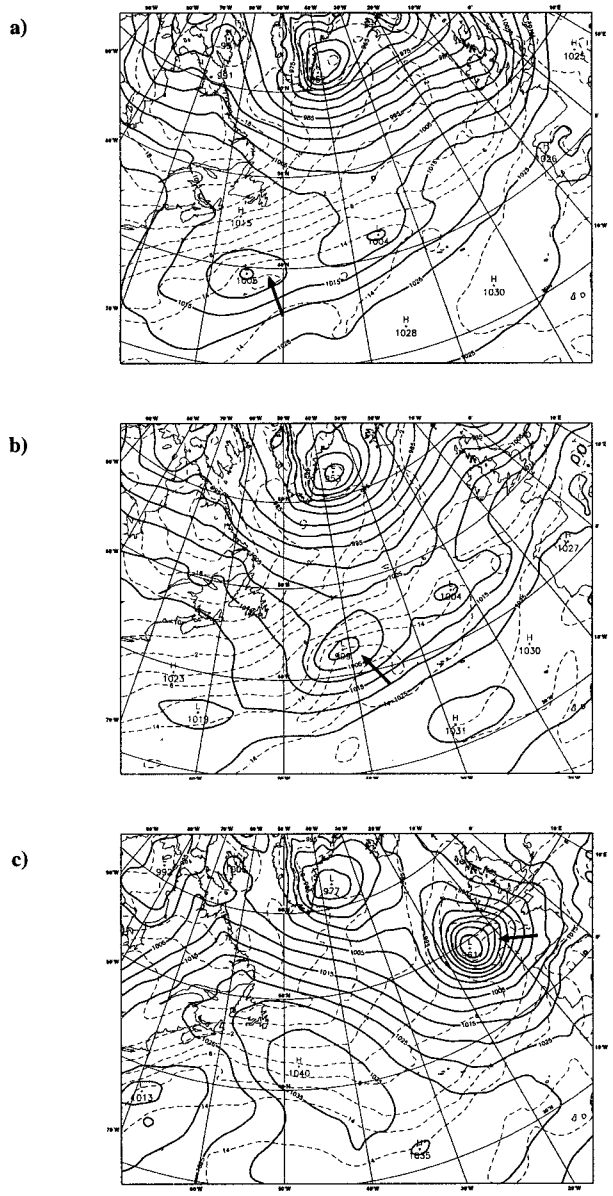

FIG. 1. ARPEGE initialized analyses (REANA): mean sea level pressure (solid) contoured every 5 hPa and 850-hPa wet-bulb potential temperature (dashed) contoured every 4 K at (a) 1200 UTC 1 Feb 1994, (b) 0000 UTC 2 Feb 1994, and (c) 0000 UTC 3 Feb 1994.

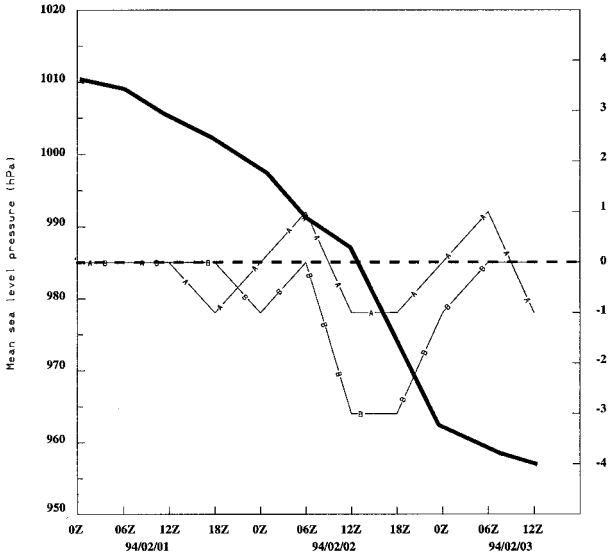

FIG. 2. Time evolution of the low pressure center as given by the REANA analysis cycle from 0000 UTC 1 Feb 1994 to 1200 UTC 3 Feb 1994 (bold line). The other curves show the MSLP difference between analyses: REANA-NOAIR (line A) and REANA-ALLAIR (line B), as discussed in section 2d.

the variation of the horizontal resolution, some characteristics of the statistical model also vary as functions of the local stretching (Cassé 1995). Information is extracted from conventional observations. The assimilation of altitude observations for analysis at time H is done within a temporal window of [H − 2 h 59 min, H + 3 h]. A quality control of the observations is performed both on the departures from the guess (a 6-h forecast issued from the previous analysis cycle, and for the current analysis time) and on the departures from an analysis made at the observation point being checked using surrounding observations. In practice, only a limited number of valid observations, as retained by the quality control, within a specified volume around each grid point are selected. This mechanism is called ''selection of observations.''

c. Interpretation tool

The main technique used to examine the results from the different experiments is a cyclone-component tracking algorithm originally developed for constructing climatological prototypes of cyclones (Ayrault 1995). The algorithm used here tracks positive maxima of relative vorticity. This definition is preferred over the classic pressure or geopotential minima as discussed by Ayrault et al. (1995, see their Fig. 8).

For a complete description of this tracking algorithm and its use in a climatological context, see Ayrault (1995). The method relies on the resolution of the association problem. The coincidence between two vorticity maxima in two successive maps (here $\Delta t = 6$ h) is established using two criteria: one tests the likelihood of the horizontal displacement under the assumptions of wind advection or classic baroclinic wave propagation; the other criterion tests the likelihood of a change in amplitude.

This method has been evaluated using ECMWF analyses against a subjective tracking at both 850 and 300 hPa for three 1-week periods, covering different large-scale types of flow over the North Atlantic. It is very successful with an input vorticity field having a resolution near T106. Moreover, it appears to be very robust

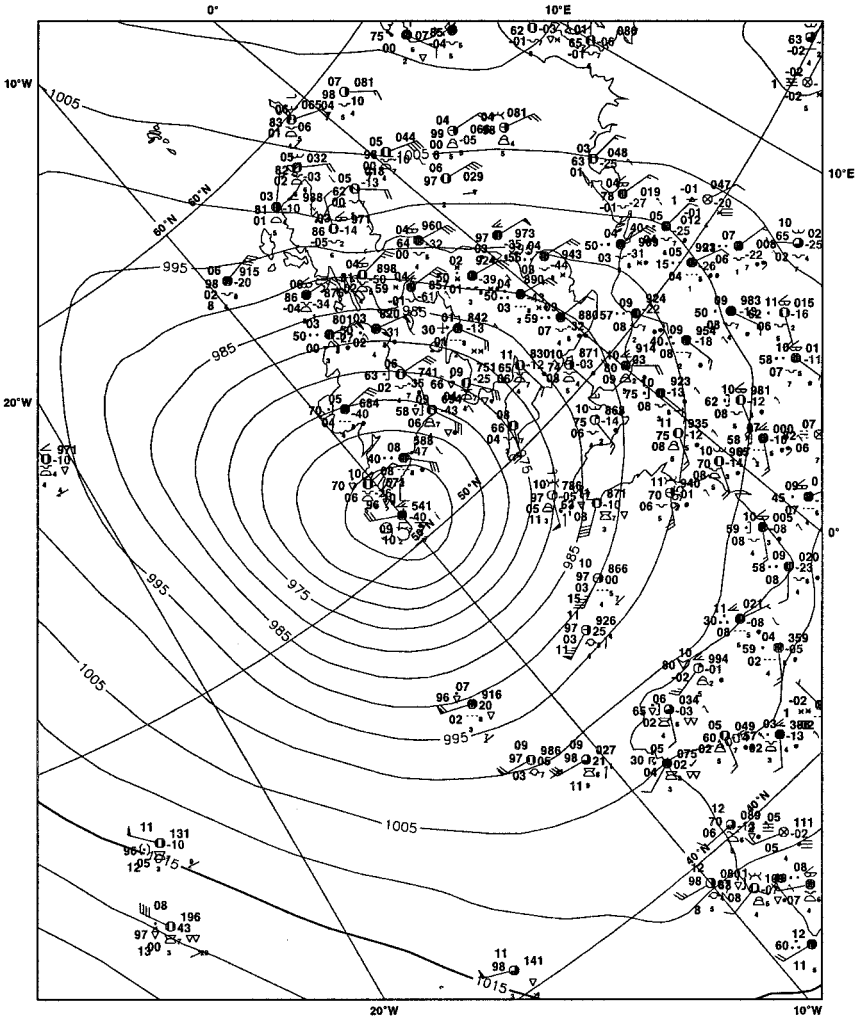

FIG. 3. Plot of SYNOP observations, and mean sea level pressure (solid lines), from the ARPEGE initialized analysis (REANA) for 1200 UTC 3 Feb 1994.

to changes in its parameters (e.g., the relative weights of the different criterion) once the resolution is chosen.

d. The three analysis cycles

All experiments are performed with the following ARPEGE/IFS configuration: the vertical discretization consists of 24 levels, and a T119 triangular field truncation is used. The horizontal stretching factor is 3.5, and the model pole is located over France. That means that the shortest resolved wave is about 48 km (T416 equivalent troncation) over France, about 100 km in the middle Atlantic, and more than 165 km (T120 equivalent troncation) west of the Great Lakes. This is sufficient for the description of the expected anomalies.

The area 0°, 120°W for the SW corner to 90°N, 10°E for the NE corner has been defined to assess the impact of the upper-level aircraft observations (Fig. 4). Three sets of experiments have been performed:

- a reference analysis of the case from 0000 UTC 29 January to 1800 UTC 3 February, called REANA, representative of the operational system;
- a second experiment without AIREP and ASDAR over the aforementionned domain, called NOAIR;
- a third one, with AIREP, ASDAR, and including U.S. ACARS data above 400 hPa, called ALLAIR. Recall that ACARS data were not included in the operational system.

Note that for these experiments, *only the wind components of aircraft observations* are assimilated. ACARS data has been handled in the same way as AIREP data.

In terms of trajectories of the 850-hPa vorticity, the three experiments are very similar, except that in NOAIR at 1800 UTC 1 February, the vorticity is 4°–5° longitude ahead of the centers in the other experiments. The final positions and values of the mean sea level

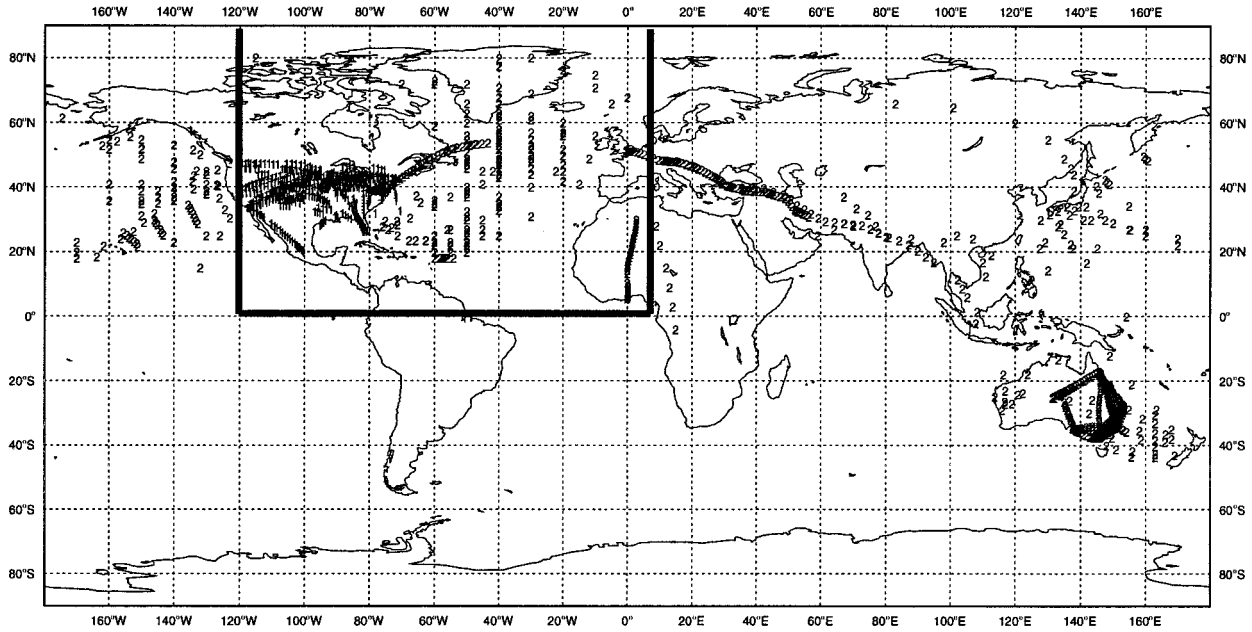

FIG. 4. AIREP (2), ASDAR (2) and ACARS (1) distributions, for 0000 UTC 29 Jan 1994. There are 677 ACARS and 1973 AIREP/ASDAR over the globe. The domain where their impact is studied is framed with bold lines (0°, 90°N; 120°W, 10°E). It contains 677 ACARS and 335 AIREP/ASDAR.

pressure of the cyclone center are very close in Fig. 5. Only the NOAIR experiment has a short westward shift of the cyclone center (less than 50 km) and a lower central pressure (956 against 957 hPa in the REANA experiment). The NOAIR cyclone is also elongated westward by a trough, but this occurs over an oceanic region without any observations to confirm this feature. The time evolution of the low centers (Fig. 2) shows differences in the rate of deepening especially for the ALLAIR experiment between 0600 UTC 2 February and 0000 UTC 3 February (a difference of 0.5 hPa h^{-1}).

An interesting time in the cyclone life cycle is the beginning of the strong deepening phase at 0600 UTC 2 February. Differences in the analyses at this time are illustrated with distributions of the PV at 330 K (Fig. 6). The differences in the analyses appear to be directly correlated, in the first place, to the position of aircraft wind observations. When present, they tend to generate smaller-scale structures in the PV distribution. It is also of interest to examine the vertical cyclone structure. Figure 7 shows the vertical velocity ω in the cross section AA′ (defined in Fig. 6e). The potential vorticity in the same plane is shown in Fig. 8. It appears that the vertical extent of the low in ALLAIR, as revealed by ω, is deeper than in REANA: ascent and especially descent zones have maxima at about 700 hPa, wheras the REANA system is kept within the upper troposphere near 400 hPa. This coincides with a stronger upper-level PV anomaly in ALLAIR (Fig. 8c), forcing a larger response that is not hindered by the presence of a low-level area of large PV [also meaning a large static stability such as in REANA (Fig. 8a)]. Note that the NOAIR upper-air fields change during analysis over the ocean, in spite of the absence of aircraft data. This is because SATEM messages are employed by this NOAIR cycle (which occur more often).

It is important to note differences also occur at low levels, even though at each analysis step only the upper levels are directly changed. These discrepancies can only come from the vertical propagation of upper-level differences (generated by the use or not of aircraft data) resulting from the 6-h model integrations, which provides the guess from one cycle to the next. In the absence of new observations (as over the ocean), the differences will continue to propagate as a result of the sequential assimilation process that is meant to preserve the memory of previous cycles. This process also operates at the level of aircraft data. Consider in Figs. 6d–f the guesses: they are already showing variations (for example, the 7-PVU area by 55°N, 37°W in NOAIR is reduced to a 5-PVU col in REANA and ALLAIR). In the absence of data in this area, these differences are still visible after the analysis (the 7-PVU strip in NOAIR is not discontinuous in the analysis while much lower PV values are confined in the other two experiments).

e. Overview of the forecasts experiments

For each set of analyses, forecasts up to 24, 30, 48, 60, and 72 h have been conducted, ending 1200 UTC 3 February 1994, when the cyclone of interest reaches Europe.

The work of analyzing and comparing these forecasts to the reference analysis REANA at the verification time

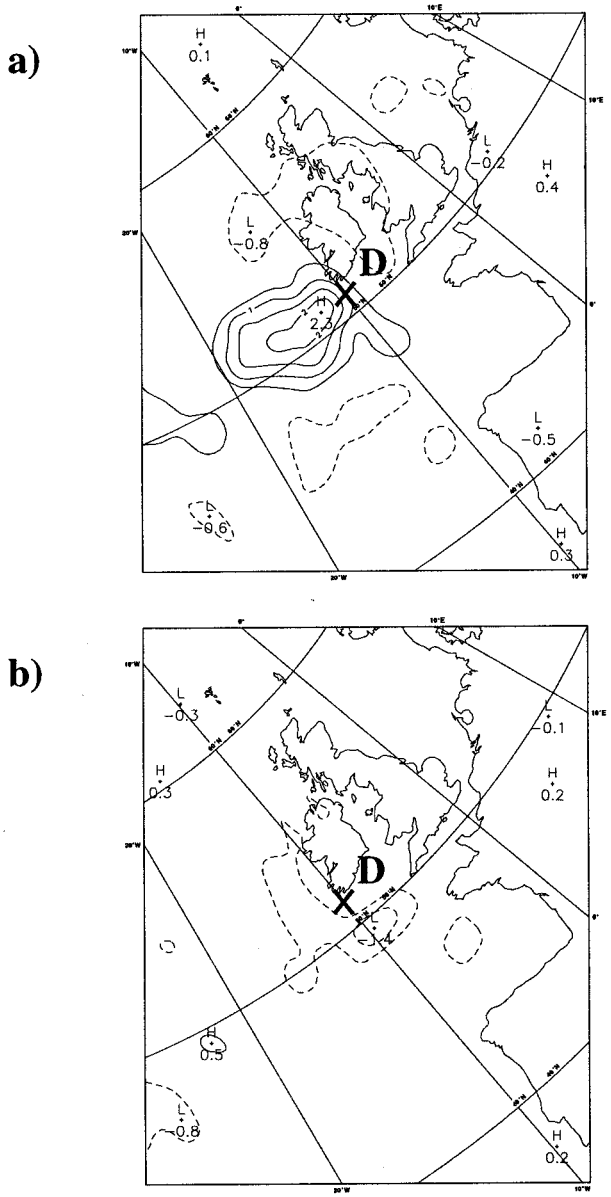

FIG. 5. ARPEGE initialized analysis for 1200 UTC 3 Feb: mean sea level pressure differences contoured every 0.5 hPa (a) REANA − NOAIR, and (b) REANA − ALLAIR. The cross corresponds to the position of the REANA cyclone center.

leads to the subjective check in Table 1, with a mark of 1 for the best forecast and 3 for the poorest. In this approach, the analysis focuses on various fields, such as the potential vorticity and upper-level jet fields, potential temperature and vorticity fields at low levels, and the surface pressure in terms of differences in structure, phase, and amplitude. Special attention is paid to mean sea level pressure since it is rather representative of the overall assessment. Two criteria are thus added to illustrate this ranking: the first one is the smallest difference among that between each of the forecast mean sea-level pressure (MSLP) minimum and REANA. The second criterion gives an idea of the spread in the forecasts, by measuring the biggest difference between them in terms of the MSLP of the low center.

From Table 1 the following comments can be made: differences in the overall forecast are generally small, aircraft observations over the North Atlantic Ocean improve the forecast, and the experiment that uses the greatest number of observation (ALLAIR) does not, in general, outperform the others. For the 48- and 30-h runs, the difference in the ranking between the REANA and ALLAIR experiments essentially comes from the development of a weak spurious trough over the North Sea, which is more intense in ALLAIR.

The distance between forecast features and the reference analysis generally decreases with the integration time length. However, it increases on this particular case at 24 h (see criterion 1): this corresponds to the time when the dynamic components linked to the development of the cyclone are in an oceanic stage in the initial conditions. For this case, the use of ACARS over the United States reduces this degradation, by downstream propagation of information.

Criterion 2 shows that a degradation of the forecast spread occurs with the short-range 30-h forecast, whereas the spread was small at 48 h. The initial conditions for this experiment (0600 UTC 2 February) have been compared above and this result shows that the differences are dynamically significant. But the most surprising result occurs for the 60-h forecasts, for which the dispersion as seen from criterion 2 is the largest. Indeed it appears that the final value of the surface pressure for the cyclone is 6 hPa deeper in the NOAIR forecast than in the two other experiments, but still 7 hPa higher than in the reference analysis (only the latter is shown in Table 1). This difference may seem small. First, note this is the worst situation provided by this case. Also, note that this is characteristic of the deepening of an ordinary frontal wave. An in-depth study of this behavior is the subject of the next two sections.

3. The dynamics of the cyclogenesis in the analyses and forecasts

The tracking algorithm of Ayrault (1995) is employed in this section in order to help construct a consistent dynamical scenario of the growth of the cyclone of interest and, at the same time, enable an insightful comparison between the 60-h forecasts.

a. Scenario derived from the reference analysis

The proper conceptual framework for an increased understanding of this case is the one that was developed by synopticians such as Sutcliffe (1947) or Petterssen (1955). It received a proper theoretical background more recently, mostly through the work of Farrell (see Farrell 1994 for an overall perspective). This framework explains cyclone development in terms of the interaction

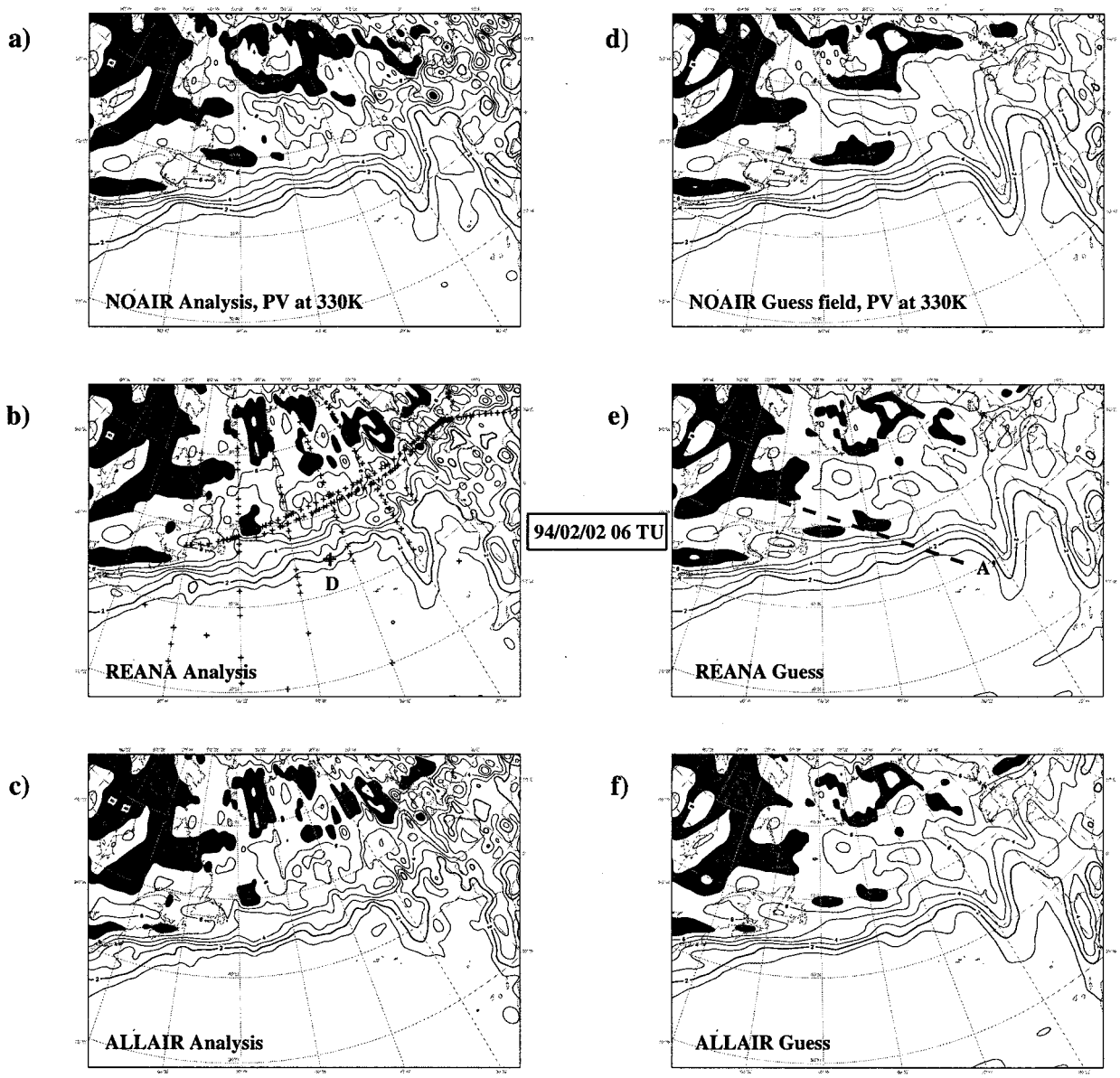

FIG. 6. ARPEGE initialized analysis for 0600 UTC 2 Feb on the 330-K isentropic surface (left), and corresponding guess (right) for the experiment NOAIR (a) and (d), reference (REANA) (b) and (e), ALLAIR (c) and (f). Potential vorticity is contoured every 1 PVU (values greater than 7 PVU are shaded). The center of the surface cyclone is plotted with a bold cross in (b). Cross-section plane AA′ for Figs. 7 and 8 is drawn in (e). The AIREP and ASDAR positions are plotted with crosses in (b).

between preexisting structures within a baroclinic area when these structures become properly phased. This is to be contrasted with the idea of waves entirely generated from unstructured noise. The point of this section is then to determine which anomalies are involved in the cyclogenesis process. Although this can be relatively straightforward at low levels, Fig. 6 suggests that this can become quite cumbersome at upper levels, since there are many anomalies present. This is where an objective tracking technique such as the one developed by Ayrault (1995) becomes useful.

Figure 9 shows the evolution of the relevant low-level vorticity maxima derived from the tracking technique. Two maxima need to be considered, noted, respectively, A (the oldest) and B. Low A forms during the first half of 30 January, and first advects in an irregular way. By 31 January, it follows a more regular eastward track. A well-organized depression is associated with it. However, its growth phase is weak and, from the second half of 1 February onward, it decays. The crucial time, for this development, is the period 0000–0600 UTC on 1 February. Low A is elongated in the west–east direction and a new vorticity maxima B emerges along its associated surface cold front, about

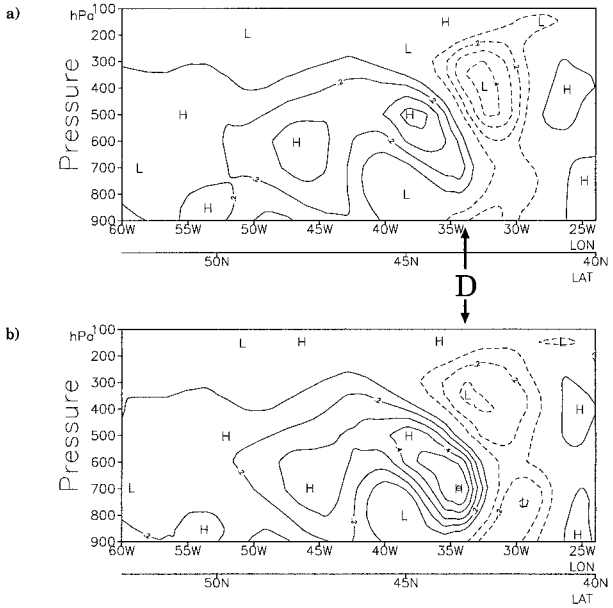

FIG. 7. Vertical cross section AA′ in ARPEGE initialized analysis for 0600 UTC 2 Feb through the cyclone vorticity maxima (AA′ are shown in Fig. 6e) (a) for the reference (REANA) and (b) ALLAIR distribution of the vertical velocity. Contours: -0.1 Pa s^{-1} ($+0.1$ Pa s^{-1}) for ascending motion (subsidence).

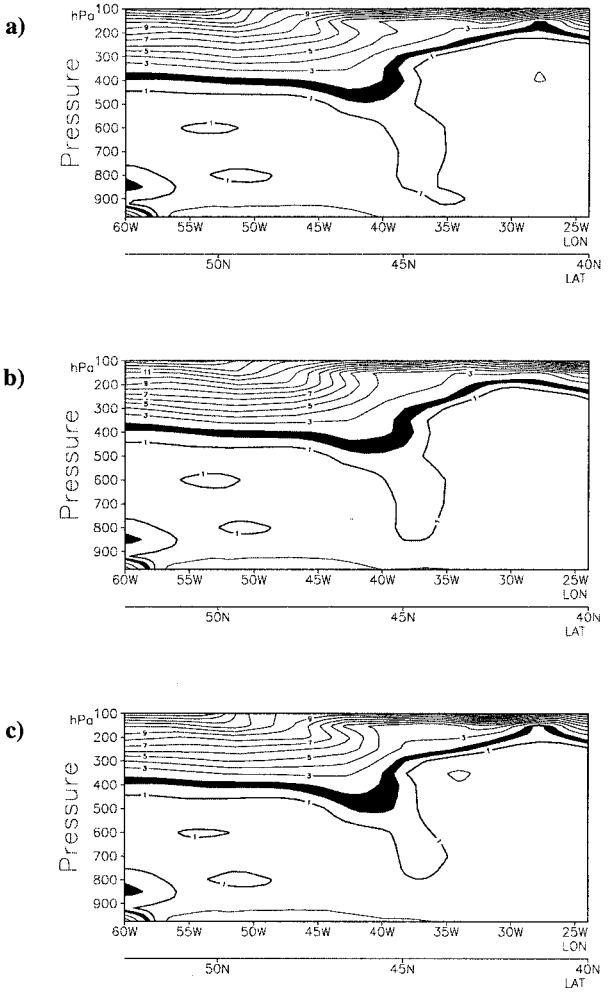

FIG. 8. ARPEGE initialized analysis for 0600 UTC 2 Feb: cross section AA′ (see Fig. 6e) of PV, contoured every 1 PVU, and shaded between 1.5 PVU and 2 PVU: (a) REANA, (b) NOAIR, (c) ALLAIR.

1300 km to the west of low A. It is this new vorticity maxima B that becomes the low of interest. The details of the formation of B is an interesting topic in itself, but it is beyond the scope of the present study.

The focus is on the subsequent development of B. We identify two stages, which are also reflected by the evolution of the low pressure center. The first stage occurs between 0000 and 1200 UTC 2 February, and it includes the most rapid increase of low-level vorticity. A short period of less rapid growth follows, and this second stage occurs between 1800 UTC and 0000 UTC 3 February. This second step corresponds to the most rapid drop of surface pressure.

The baroclinic amplification framework can explain these two phases providing preexisting anomalies can be identified at upper levels. The other factors to be considered are the baroclinic zone itself (as represented, e.g., by the jet stream), the horizontal projection of the vertical shift between the upper- and low-level components, and representation of the most critical vertical tilt, parallel to the thermal wind. The work of Warrenfeltz and Elsberry (1989) stresses the importance of having precursor structures with comparable amplitudes for rapid development. The minimal amplitude required is

TABLE 1. Subjective assessment of forecasts, classified from 1 (the best) to 3 (the poorest), as compared to the reference analysis REANA. This assessment combines several aspects, two of them are shown, additionally, on the table. A first criterion shows the smallest difference between each forecast low pressure center value and the REANA analysis. A second criterion shows the largest difference between the three pairs of forecasts that can be constructed.

Integr. time (h)	REANA	NOAIR	ALLAIR	Crit. 1	Crit. 2
72	2	3	1	−13	1
60	2	1	3	−7	6
48	1	3	2	−6	1
30	1	3	2	−1	2
24	2	3	1	−2	1

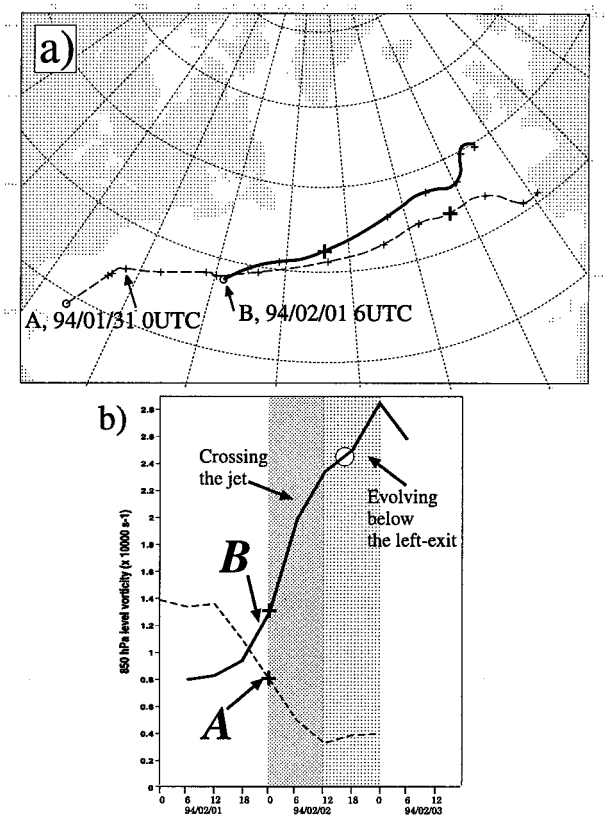

FIG. 9. (a) Trajectories of the 850-hPa vorticity centers from the REANA analysis, starting 0600 UTC 30 Jan. Crosses are set every 6 h. (b) Time evolution of their amplitude. Vorticity is in units of 10^{-4} s^{-1}. Note the two low-level precursors A and B. Bold crosses correspond to the position of the vorticity centers at 0000 UTC 2 February 1994.

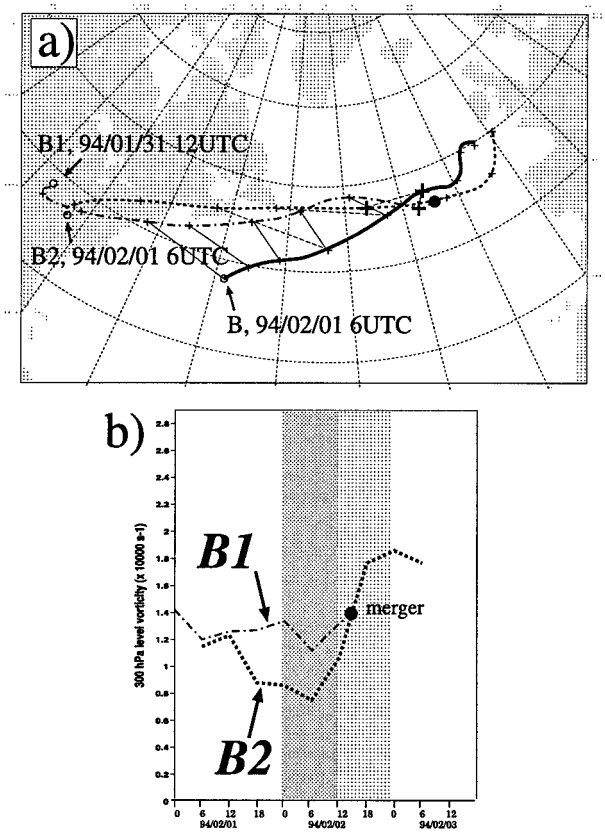

FIG. 10. (a) Trajectories of the 300-hPa vorticity centers (ULV) and the 850-hPa vorticity center (LLV) from the reference analysis (REANA), plotted every 6 h. Bold crosses correspond to the respective positions at 1200 UTC 2 Feb. (b) Time evolution of the two upper-level centers (ULV). Curve B_1 corresponds to the ULV starting at 1200 UTC 31 Jan, curve B_2 to the ULV starting at 0600 UTC 1 Feb.

obtained by B during its slow growth period (call it phase 0) on 1 February. Warrenfeltz and Elsberry also show that the organization of the jet in the form of a streak enables it to behave like an upper-level anomaly that rapidly repositions the low toward its ''left exit'' or northeastward end. Other elements that can play a role in these interactions are the change of tilt normal to the thermal wind and the merging of two upper-level anomalies (Hakim et al. 1995).

Several tracks of upper-level anomalies can be identified at 300 mb. Combining them with maps depicting the baroclinic zone and the surface anomalies, two of them turn out to be involved in the evolution studied here (Fig. 10). The first stage of the growth of B starts with the combination of the northward crossing of the baroclinic zone and the baroclinic interaction with a first upper-level anomaly called B1. The tracking algorithm follows positive vorticity maxima only. However, the study of upper-level maps shows that this anomaly is closely related to a mobile jet streak of about 95 m s^{-1} embedded within a zone with an average value between approximatly 60 and 70 m s^{-1}. As shown by the weak growth of B1, the contribution of the baroclinic interaction to the overal development is small compared to that of shifting B toward the left exit. The small impact of the baroclinic interaction on the upper-level component in the presence of a jet streak is noted by Warrenfeltz and Elsberry. Note that the drop in the amplitude of B1 between 0000 and 0600 UTC on 2 February remains to be understood.

The second stage of the growth of B involves a new upper-level anomaly (B2) that crosses the Atlantic very quickly (about 50 m s^{-1}) and does benefit from baroclinic interaction with low B (and perhaps from the large shear along the jet). Anomaly B2 actually overtakes B1, and they merge together between 1200 and 1800 UTC 2 February. This also increases the strength of the upper-level jet in the eastern Atlantic. During this time period, the low benefits from the ageostrophic circulation that accompanies the left-exit region (see Fig. 11) in which it remains embedded for 18 h (since 0600 UTC 2 February). It also benefits from the merging that reinforces the upper-level vorticity component. After 0600 UTC 3 February, the low drifts away from the baroclinic zone toward the north. The interaction weakens and many

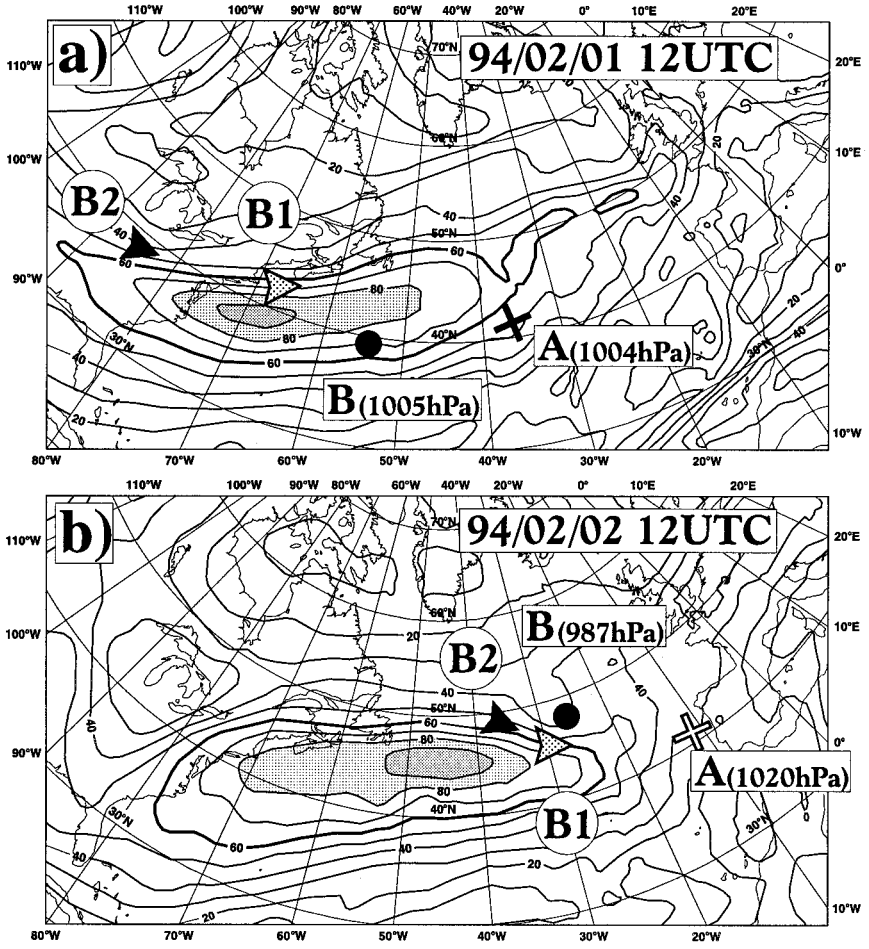

FIG. 11. Evolution of the main dynamical components of the case as shown by the reference (REANA) ARPEGE initialized analysis for (a) 1200 UTC 1 Feb, and (b) 1200 UTC 2 Feb. Solid lines correspond to the 330-K wind intensity contoured every 10 m s^{-1}, highlighted for 60 m s^{-1}, and shaded above 80 m s^{-1}. The black point (black cross) indicates the position of the surface cyclone center B (A). The black arrow (dot arrow) stands for the B_2 (B_1) upper-level vorticity anomaly.

cyclogenesis parameters show signs of decay or decrease.

In summary, low B develops through successive baroclinic interactions with two upper-level structures in a finite-length baroclinic zone. The linear effects or direct energy conversion from the baroclinic interaction between vorticity maxima seem, however, not as important as less linear effects due, in the first stage, to the shifting of B toward the northeast end of a large jet streak and, in the short second stage, to the reinforcement of the upper-level component by the merging of B1 and B2. It should be pointed out that no low-level-driven process can match in strength the various forms of baroclinic interaction involving some form of coupling with upper levels (Joly 1995; Ayrault 1998). The fate of low A illustrates what happens, along the same baroclinic area, in the absence of any significant upper-level anomaly: no development takes place. The importance of upper levels on the dynamics of the system contrasts with the dynamics of differences, as will be discussed in section 4.

b. Development scenarios in the 60-h forecasts

The description of the cyclogenesis using the methods employed in the previous section can now be applied to some of the 60-h forecasts. The low-level trajectories for the REANA and NOAIR forecasts are shown in Fig. 12. The key predictability problem in this type of situation is to determine which low-level vorticity maxima, and associated ascent and cloud system, will develop. The NOAIR forecast picks the wrong one: it develops the vorticity center A after 30 h, while REANA develops B, 6 h earlier (Figs. 12c and 12d) and 10° more to the west. This example shows that the upper-air aircraft data lead to a crucial difference in the depiction of the life cycle of a cyclogenesis event as seen at low

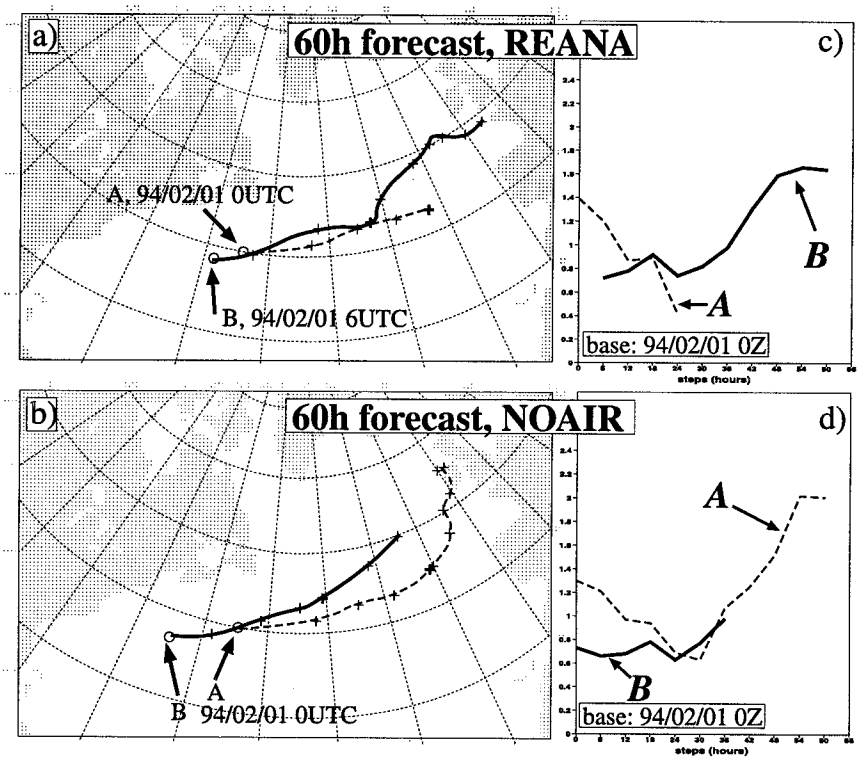

FIG. 12. (a) and (b) Same as Fig. 9a, (c) and (d) same as Fig. 9b but for forecast runs: (a) and (c) REANA 60-h forecast, (b) and (d) NOAIR 60-h forecast. Bold crosses correspond to the position of the vorticity centers after 24 h of simulation (0000 UTC 2 Feb).

levels, even though the final difference in the pressure field appeared to be modest.

It is important, however, to temper this conclusion by examining the evolution simultaneously at upper and low levels. It turns out, in fact, that *all* 60-h forecasts are unable to handle the proper cyclogenesis scenario. These errors, common to the three forecasts, are now presented using the REANA experiment only.

The first stage of growth, when the surface vorticity begins its northward crossing of the jet, takes place more than 12 h later than in the analysis. This is shown by the growth curves in Fig. 12. The combination of upper and low levels (Fig. 13) also clearly shows that the low-level cyclogenesis component crosses the upper-level one at 20°W (REANA forecast) or 13°W (NOAIR forecast) instead of 30°W (in the analysis). The second stage, which follows the merging of the two upper-level precursors, simply does not take place in the simulation. The net result is a significant underestimation of vorticity growth. The reason for this is that the forecasts do not distinguish between B1 and B2: they handle only one upper-level precursor (whose trajectory is closer to B1 than to B2).

The automatic tracking makes the documentation of the differences between forecasts or between analysis and forecast over a complete life cycle relatively easier. It remains to be understood why two rather close analyses (such as REANA and NOAIR) can lead, with the same model, to two very different life cycles of the low.

4. Detailed study of the 60-h forecast using dynamical diagnostics

The main question addressed here is: what are the differences in initial conditions that lead to these different scenarios in the 60-h forecasts? This approach is different than the one consisting of understanding the forecast error identified by comparison with a ''true'' solution—such as observations, analysis (see, e.g., Rabier et al. 1996). Here, the two forecasts have their own forecast errors (in the previous sense), whose origins could be locally the same. But the aim of this study is to try to understand the differences in initial conditions that leads to one forecast solution (even imperfect) rather than the other. The origins of the divergence can be inferred by examining differences in the cyclone precursors (e.g., PV anomalies) or in the growth of unstable structures of analysis errors. In order to understand the different behaviors of the development in the 60-h forecasts resulting from the different analysis cycles, two approaches will be employed. The first step is to determine some kind of educated guess derived from the tracking algorithm that will relate the differences of behavior at low levels to the way upper levels are handled

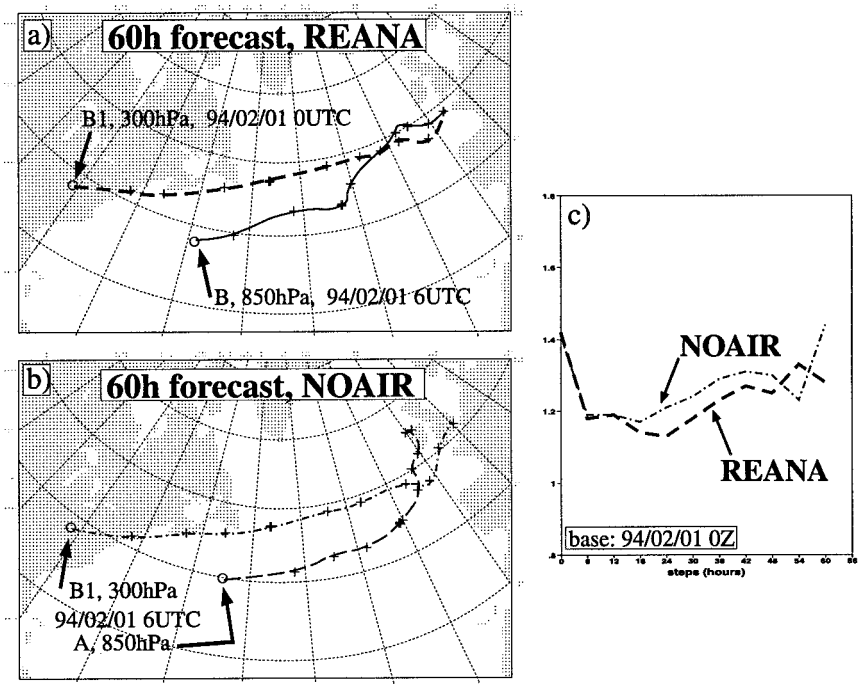

FIG. 13. (a) and (b) Trajectories of the 300-hPa vorticity center (ULV) and the 850-hPa vorticity center (LLV) from the 60-h forecasts: (a) REANA, (b) NOAIR, plotted every 6 h. Bold crosses correspond to the respective positions after 24 h of simulation. (c) Time evolution of the 300-hPa vorticity anomaly (ULV) of the REANA (dashed curve) and NOAIR (chain-dot curve) 60-h forecasts ($\times 10^4$ s^{-1}).

in both 60-h forecasts and from there to the observations. The resulting finding, as it turns out, only provides part of the solution. The second step is to try to isolate the dynamically important differences between the initial states for this particular change in the 60-h forecast solution using the adjoint technique. It will be shown that it becomes relatively easy to find the starting point of model divergence in the assimilation cycle.

a. Explaining upper-level differences: The direct effect of upper-level observations

From Figs. 12 and 13, it appears that A is sustained in the NOAIR forecast as a result of its location beneath the exit area of the upper-level jet after 30 h of simulation, where it then deepens due to the ageostrophic, and cyclogenetic, circulation. During the first 30 h, the amplitude of B evolves in approximately the same manner in both simulations. However, B begins crossing the upper-level jet earlier in the NOAIR simulation. The interaction between the single upper-level vorticity anomaly and B exists in both forecasts. But in the NOAIR case, their respective positions begin to be cyclolytic around hour 30, and in an area—the cold side of the jet away from the exit region—where there is no other dynamical structures to allow further increases in strength. The stronger intensity of the upper level vorticity anomaly in NOAIR after 12 h probably leads to this different development of B. Also a different evolution of nonlinearity in both simulations modifies the system phase speed. As a result, the difference in the time evolution of the 300-hPa vorticity center was investigated. Its location and development were followed backward in time (with a manual tracking method) and then identified in the initial conditions.

The initial difference in the wind speed with respect to the location of the upper-level PV dipole reached 7.8 m s^{-1} on the 330-K surface, in the center of a wind anomaly with a diameter of approximately 10°, situated between 100 and 450 hPa. After some examination of the data assimilation algorithm, it was found that this initial difference resulted from a different use of the 300-hPa zonal wind (82.6 m s^{-1}) component of the TEMP message issued by the upper-air station of Charleston, South Carolina, located at 33°N, 80°W. This observation has been included in NOAIR but not in the REANA analyses used for the 60-h forecasts due to difference in the criterion of the quality control selection. It is ultimately due to the impact of the previous analysis cycle on the guess fields. In order to verify this conclusion, this wind observation was removed from the NOAIR analysis. A new 60-h forecast (NOAIRBLACK) was then run using this modified analysis. The effect of the modification in the NOAIRBLACK initial condition is a local decrease of the wind of about 7.1 m s^{-1} on the 330-K surface compared to the NOAIR

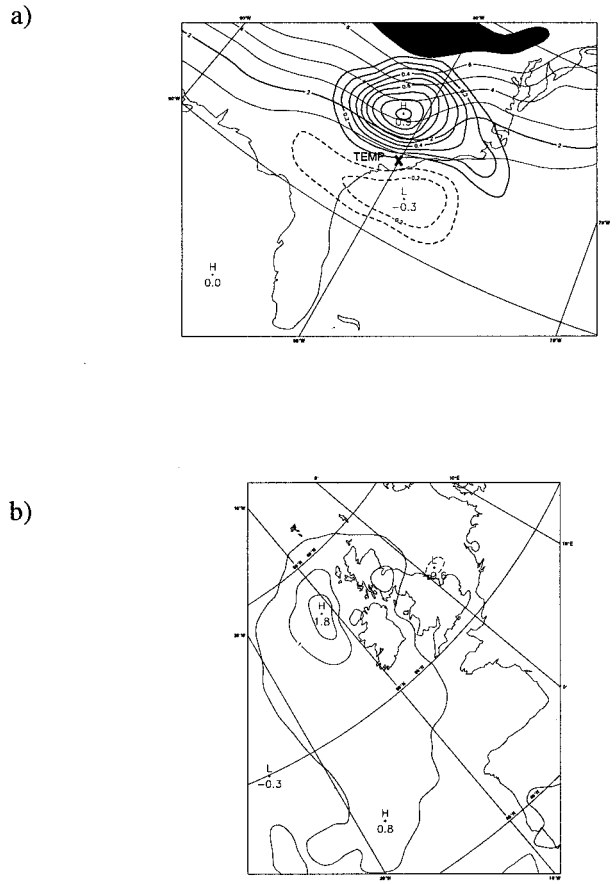

FIG. 14. (a) Potential vorticity on the 330-K surface (contoured every 1 PVU and shaded above 7 PVU) for the NOAIR analysis at 0000 UTC 11 Feb, with the PV anomalies (bold dash and solid lines, contoured every 0.1 PVU) resulting from removing the 300-hPa zonal wind component of the 33°N, 80°W TEMP message. (b) MSLP difference field (NOAIRBLACK − NOAIR) after 60 h of simulation (1200 UTC 3 Feb) contoured every 0.5 hPa, resulting from removing only this observation.

analysis. The residual is caused by the difference between guesses. The new forecast features an attenuated deepening of the surface pressure as expected (Fig. 14b), but by only 1 hPa (965 against 964 hPa for the center) instead of 6 hPa. However, the cyclogenesis scenario proposed by the 60-h NOAIRBLACK forecast remains close to the NOAIR one (the development of the surface wave A instead of B remains). Even if this observation brings the two 60-h forecasts nearer, at the final time, it does not explain the different forecast scenarios.

b. Adjoint method

Faced with the relatively large number of degrees of freedom in the differences in the initial conditions, the kind of approach performed in previous subsections may become impractical. Therefore it was decided to apply adjoint equations to this problem, the question addressed being: to which aspect of the differences between REANA and NOAIR analyses is the divergence between the two 60-h forecasts most sensitive. Adjoint equations for mapping sensitivities are used by Hall et al. (1982), Errico and Vukicevic (1992), and Rabier et al. (1992). An introduction of this approach is presented in Errico (1997). The following notations are defined according to the ones used by Errico.

Let J be a scalar measure of the 60-h forecast difference between REANA and NOAIR. The method is to compute the sensitivity fields with respect to the initial conditions at t_0, that is, $\partial J/\partial a$, where a can be any of the model variables: in this case, we use vorticity ζ, divergence D, temperature T, and surface pressure p_s. The model employed (B) as well as its linear tangent (B') are global, spectral, truncated at T119 with 24 hybrid levels and without any geometrical stretching of the sphere.

Here, B' includes parameterizations of only horizontal and vertical diffusion and surface drag. The trajectory $b = B(a)$ with respect to which the linear computations are performed is the REANA forecast experiment, with full physics. The diagnostic function J, in this case, measures the divergence between the two 60-h forecasts. It is expressed as the integral over the square of the sea level pressure P difference between the 60-h forecasts derived from REANA and NOAIR:

$$J(T, D, \zeta, p_s) = \frac{1}{\Sigma} \int \int_{\Sigma} a[p_s - P_{\text{REANA}}(t1)]^2 \, dx \, dy$$

$$a = \frac{R_a T_R}{g P_R} \begin{cases} T_R = 300 \text{ K} \\ P_R = 800 \text{ hPa} \end{cases}$$

$$p_s = P_{\text{NOAIR}}(t1),$$

where $t1$ is 1200 UTC 3 February and Σ is the area extending from 20°W to 0°E, and from 40° to 60°N. The gradient of J is computed for the canonical scalar product. This means that the sensitivity fields at t_0 will point out areas where initial perturbations (difference between REANA and NOAIR analyses) may have a large effect (positive or negative) on the difference between the two 60-h forecasts. Because the divergence term (D) is an order of magnitude smaller than the temperature and vorticity terms (Rabier et al. 1992), only the sensitivity fields with respect to T, ζ, and p_s at the initial time are studied.

What kind of information is given by these sensitivity charts? The gradient of J with respect to the initial condition is plotted in Fig. 15 for the vorticity at 850 hPa. There are two noteworthy points. First, differences in the initial conditions at low levels may have an effect on the divergence between the two forecasts, and areas of significant sensitivity are quite large. For example, sensitivities exceeding one-half the maximum amplitude extend from 90°W to 0° between 20° and 65°N (Fig. 15). Second, these sensitivity structures cover a domain larger than the one that contains all the dynamical com-

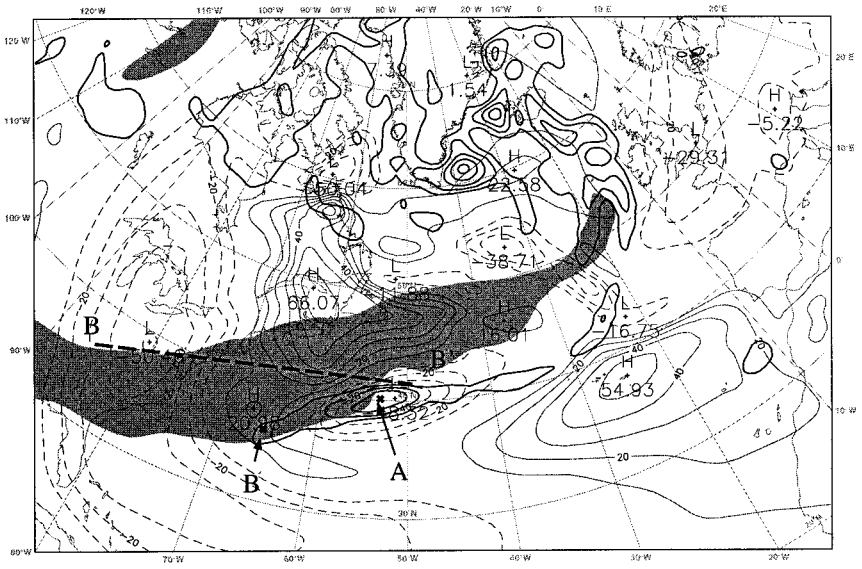

FIG. 15. Fields of sensitivity with respect to initial vorticity (solid and dash lines contoured every 10 units, scaling by 10 000) at 850 hPa 0000 UTC 1 Feb. Superimposed are the REANA absolute vorticity analysis (bold lines contoured every 5 10^{-5} s^{-1} above 15 10^{-5} s^{-1}) at 850 hPa, and the 300-hPa jet (shaded above 60 m s^{-1}).

ponents of the cyclogenesis. This highlights the idea that another factor interposes itself in reconstructing a scenario of a meteorological event: the dynamics of analysis errors. They are able to amplify relatively independently of the cyclogenesis dynamics, in the same sense and the same limitations that two cyclogenesis events occurring at the same time in the same broad area are independent from one another.

These sensitivity areas move slightly westward with altitude [as mentioned in many papers as a baroclinic tilt of the gradient; see Rabier et al. (1992), e.g.]. The amplitude of the maxima and minima of vorticity sensitivity fields depends little on the vertical level. On the contrary, the temperature sensitivity fields are more intense near 700 and 600 hPa. At these levels, their horizontal extension is limited between 80° and 30°W, and between 35° and 55°N. Their structures are sharper than the ones of the gradients with respect to vorticity. Some structures of the sensitivity fields have a length smaller than 300 km. They are collocated with precursors of the dynamical structures of the 60-h forecast cyclogenesis [i.e., above the two low-level vorticity centers (Fig. 15)]. Others that have larger vertical and horizontal extensions are associated with the dynamics of large-scale structures, such as the upper-level jet.

In a first stage of interpretation of the gradients, the impact of removing the previously discussed TEMP 300-hPa wind component is discussed. The PV anomaly (shown in Fig. 14a) resulting from this one observation projects itself on temperature and vorticity fields in the following way: the use of the wind component in the NOAIR analysis leads to a local cooling and to a local increase of the vorticity north of the TEMP location and to heating and decrease of the 300-hPa vorticity south of it (not shown). As in Errico (1997), the impact of an anomaly on J could be canceled if it covers a sensitivity region with both positive and negative areas. This is the case here for the temperature anomalies at 300 hPa. However, the negative vorticity anomaly south of Charleston contributes to an increase of J, which means an increasing difference between REANA and NOAIR forecasts. Indeed, using the NOAIRBLACK run for an explicit computation of J in both cases gives $J_{\text{NOAIR}-\text{REANA}} = 430$ J and $J_{\text{NOAIRBLACK}-\text{REANA}} = 381$ J. Note that the last J stands for joules, the unit of our function J. This one observation leads to a 11% change in the MSL pressure difference.

c. *Sensitivity times perturbation and resulting findings*

As a consequence of the linearization, the net change of J is given by the sum of the separate change $(\partial J/\partial a)\delta a$, where a could be ζ, T, D on each level, or Ps. In our approach, δa is the difference between the two initial conditions (REANA and NOAIR analysis). This perturbation is the full difference resulting from whether or not the upper-level wind aircraft data over the North Atlantic Ocean are used after 3 days of assimilation. The important components of this difference field (δa) can be isolated by computing their product with the sensitivities ($\partial J/\partial a$). The resulting maps are now discussed.

The gradients are controlled by the dynamics of the problem (as represented by the equations and trajectory of the tangent-linear model) while the differences de-

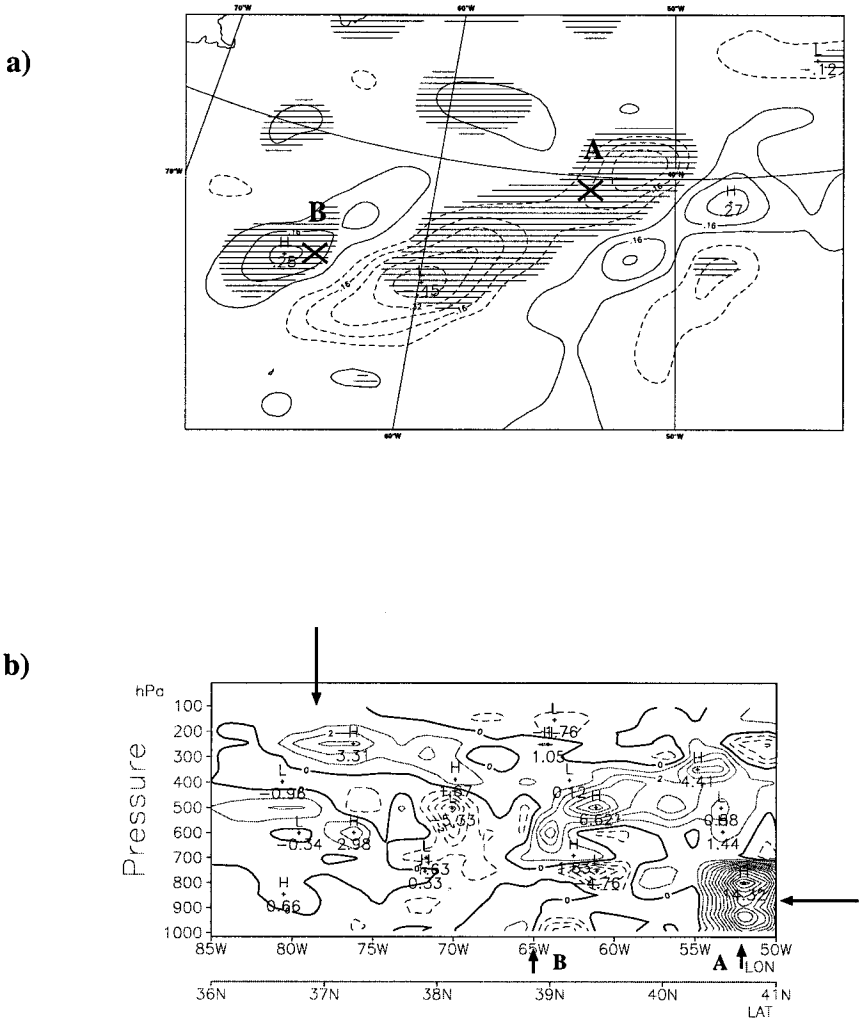

FIG. 16. (a) Diagnostic $(\partial J/\partial\zeta)\delta\zeta > 0$ for initial condition: 0000 UTC 1 Feb at 850 hPa (hatched area), vorticity differences NOAIR − REANA (solid and dash lines contoured every 0.08 10^{-5} s^{-1}). (b) Cross section BB′ (cf. Fig. 15) for the field $(\partial J/\partial\zeta)\delta\zeta + (\partial J/\partial T)\delta T$ contoured every 1 unit.

pend primarily on the error structure function as well as, to some extent, the dynamics of the previous days through the assimilation cycle. Because of these differing sources of information, relatively simple differences between analyses have a complex impact on the changes of *J*. The combination of the wave along the cold front (at 45°N, 25°W) with the sensitivity fields is an example.

The positive areas of the product $(\partial J/\partial a)\delta a$ are now considered, since they are the active differences contributing to the forecast divergence. The objective here is to identify how these differences have been introduced in the analysis. The vicinity of the baroclinic region is investigated. At upper levels, the main active differences are dominated by the vorticity component in three preferential areas: the warm side of the entrance region of the upper-level jet, both sides of the exit region, and over the trough associated with the primary cyclone and located over northwestern Europe. At 850 hPa, the diagnostic $(\partial J/\partial T)\delta T > 0$ highlights two main structures: the above-mentioned wave along the cold front, and the two low-level vorticity centers A and B. A look at the diagnostic $(\partial J/\partial\zeta)\delta\zeta > 0$ at the same level also indicates positive structures in the vicinity of these vorticity centers (Fig. 16a). Active differences are identified on the temperature, west of the vorticity center A, with a relative cooling in NOAIR at 40°N, 61°W, and on the vorticity field above A and B.

d. The selection of observations

Section 2 showed that, thanks to the assimilation cycles, differences at low levels can develop as a result of the propagation of information from aircraft observations concentrated at upper levels. It is noteworthy

that the most significant differences, in terms of the ''success'' of the 60-h forecast, are located at 850 hPa. Using the gradients computed for J, the question of the source of the ''active'' difference above A and B at 850 hPa can be examined. It appears that the source is entirely due to the previous stages of the assimilation cycle. Indeed, two cycles earlier (or 12 h sooner), at 850 hPa, a humidity observation from a relatively isolated TEMP station (Bermuda), located at 32.4°N, 64.7°W, has been introduced into the NOAIR analysis, but not in the REANA one. The origin of this discrepancy is the quality control criterion that compares observations to the background. This is how, quite suddenly, a significant difference is brought down to lower levels, as a consequence of the previous cycles. The consequence of this differential selection of observations is a relative drying of about 40% in the NOAIR analysis south of the two surface lows, compared with the REANA analysis. This initially spherical perturbation is rapidly carried downstream and stretched by the low-level circulation, especially the low-level jet upstream of the surface lows. This humidity perturbation impacts, through the physical parameterizations during the next two cycles, the dynamical background fields, in particular the temperature and the low-level jet intensities, and therefore the vorticity field.

It is noteworthy that the ALLAIR analysis checking leads to the same choice as in the NOAIR one. Nevertheless, after 12 h of assimilation, differences between REANA and ALLAIR decrease, especially in the cold air behind the surface wave A. This feature is associated with a similar selection process for the 300-hPa zonal wind component of the Charleston TEMP data for both experiments, and may explain why the 60-h forecast of the ALLAIR experiment does not depart from REANA as much as from NOAIR. The use of a larger set of aircraft observations supplies analyses with information that may correct, through the assimilation cycles, the errors caused by the selection of an erroneous observation.

A further aspect of the active differences must be mentioned by returning to the vertical structure of the difference fields. A cross section BB′ (Fig. 16b, axis plotted in Fig. 15) through the upper and lower components of the perturbations of the vorticity fields reveals that the differences have a baroclinic tilt. This ''baroclinic shape'' error will entirely contribute to the divergence between the forecasts. The two sources of discrepancies studied in this section appear in Fig. 16b: the impact of the 300-hPa wind perturbation and the indirect impact (on ζ and T) of the selection of the 850-hPa humidity observation. The selection of an observation is particularly crucial if it occurs in a dynamically unstable region. In such a region, the slightest perturbation may change the scenario of the development.

5. Conclusions

The impact of the upper-level wind aircraft data has been presented using the analyses and forecasts of a predictable classic baroclinic development over the North Atlantic Ocean. It takes place well out to sea, over a data-sparse area. The continuous supply of upper-level aircraft data through the assimilation cycles allows modifications of the dynamically important structures. Information is transmitted to the lower levels within less than 3 days, after having been confined during the first assimilation cycles to upper levels, in a complicated way by combining the dynamics and the observation selection process. This modified vertical structure leads to significant forecast differences.

A simple diagnostic was defined, using the adjoint method, to extract active differences for improvement of the forecast, at least for its adiabatic part. Over the baroclinic area, this diagnostic leads to the identification and study of the origin of two active differences. They originate from the handling of TEMP messages, one at 300 hPa and one at 850 hPa. The aircraft data assimilation, by modifying the 6-h forecast used as a background of the next analysis step, modifies the evaluation of some criteria in the control quality mechanism, for other kind of observations, such as TEMP. Such differences may amplify as the time integration proceeds, as is the case here, especially for the low-level one. There is a contrast to be noted between the dynamics of the cyclone and that of the amplification of the low-level difference. Both take advantage of the baroclinic zone (and in this sense, influence one another), but the cyclone evolves like a Pettersen type-B development while the difference grows up from low levels.

It was shown that the selection of an observation is crucial in dynamically unstable regions. In such areas, the slightest perturbation may change the scenario of development. The consequences of the selection are accentuated over data-sparse areas since errors amplify, unchecked, from one assimilation cycle to the next.

Although this case had been relatively well forecasted by the operational ARPEGE model, improvement is still possible. Indeed we show that the upstream addition of ACARS data over the United States improves the T + 72-h forecast and attenuates the weakness of the T + 24-h forecast when the system is in an oceanic stage.

This 60-h forecast set illustrates that a forecast may be synoptically good but still dynamically wrong, by having a completely different cyclogenesis scenario from the observed one. An automatic tracking algorithm allows this type of result to emerge in a simple and objective manner. Such a tool, primarily developed for climatological purposes as well as for the planning of the FASTEX experiment, could lead to at least two other applications in the field of the numerical weather prediction. One is a different kind of scoring that would measure the ability to predict specific cyclogenesis events rather than non descript errors. The other is to combine numerous tracks at various forecast ranges and bring out a new category of systematic errors in models.

Acknowledgments. The authors wish to thank the ARPEGE assimilation team (Météo-France/CNRM/GMAP) for its support and comments, especially Jean Pailleux, Vincent Cassé, and Philippe Caille. Thanks to Claude Fischer, Philippe Arbogast, and Gerald Desroziers for their helpful answers. The authors gratefully acknowledge Aaron Boone for his advices and corrections to improve the language of the text and the anonymous reviewers for helping us focusing the original manuscript.

REFERENCES

Ayrault, F., 1995: Suivi automatique des tourbillons sur l'atlantique nord. D.E.A. M.S. thesis, Université P. Sabatier, 30 pp. [Available from Université Paul Sabatier, 118 Route de Narbonne, 31062, Toulouse, France.]

——, 1998: Environnement, structure et évolution des dépressions météorologiques: réalité climatologique et modèles types. Doctorat de l'Université P. Sabatier, 328 pp. [Available from Université Paul Sabatier, 118 Route de Narbonne, 31062, Toulouse, France.]

——, F. Lalaurette, A. Joly, and C. Loo, 1995: North Atlantic ultra-high frequency variability: An introductory survey. *Tellus,* **47A,** 671–696.

Bell, R., N. Ingleby, and C. Parrett, 1994: Processing and assimilation of automated aircraft data. UKMO Forecasting Research Division Tech. Rep. 81, 25 pp. [Available from Meteorological Office, London Road, Bracknell, Berkshire RG12 2SZ, United Kingdom.]

Brewster, K., S. Benjamin, and R. Crawford, 1989: Quality control for ACARS meteorological observations—A preliminary data survey. Preprints, *Third Int. Conf. on the Aviation Weather System,* Anaheim, CA, Amer. Meteor. Soc., 124–129.

Cassé, V., 1995: Data assimilation at METEO-FRANCE. *Extended Abstracts, Second International Symposium on Assimilation of Observations in Meteorology and Oceanography,* WMO/TD No 651, Vol. II, 433–435.

Courtier, P., and J.-F. Geleyn, 1988: A global spectral model with variable resolution. Application to the shallow water equations. *Quart. J. Roy. Meteor. Soc.,* **114,** 1321–1326.

——, C. Freydier, J.-F. Geleyn, F. Rabier, et M. Rochas, 1991: The ARPEGE project at METEO-FRANCE. *ECMWF Seminar Proc., Workshop on Numerical Methods in Atmospheric Models,* Reading, UK, ECMWF, 193–231.

Errico, R., 1997: What is an adjoint model? *Bull. Amer. Meteor. Soc.,* **78,** 2577–2591.

——, and T. Vukicevic, 1992: Sensitivity analysis using an adjoint of the PSU–NCAR mesoscale model. *Mon. Wea. Rev.,* **120,** 1644–1660.

Farrell, B., 1994: Evolution and revolution in cyclogenesis theory. Preprints, *Symp. on The Life Cycles of Extratropical Cyclones,* Vol. I, Bergen, Norway, University of Bergen, 101–110.

Graham, R., 1994: Routing monitoring of data impact on forecasts using case study methods. *Preprints, 10th Conf. on Numerical Weather Prediction,* Portland, OR, Amer. Meteor. Soc., 48–50.

Hakim, G., L. Bosart, and D. Keyser, 1995: The Ohio Valley wave-merger cyclogenesis event of 25–26 January 1978. Part I: multiscale case study. *Mon. Wea. Rev.,* **123,** 2663–2692.

Hall, M. C., D. C. Cacuci, and M. Schlesinger, 1982: Sensitivity analysis of a radiative–convective model by the adjoint method. *J. Atmos. Sci.,* **39,** 2038–2050.

Heming, J., 1990: The impact of surface and radiosonde observations from two Atlantic ships on a numerical weather prediction model forecast for the storm of 25 January 1990. *Meteor. Mag.,* **119,** 249–260.

Hoskins, B., M. McIntyre, and A. Robertson, 1985: On the use and significance of isentropic potential vorticity maps. *Quart. J. Roy. Meteor. Soc.,* **111,** 877–946.

Joly, A., 1995: The stability of steady fronts and the adjoint method: Nonmodal frontal waves. *J. Atmos. Sci.,* **52,** 3082–3108.

——, and Coauthors, 1997: The Fronts and Atlantic Storm-Track Experiment (FASTEX): Scientific objectives and experimental design. *Bull. Amer. Meteor. Soc.,* **78,** 1917–1940.

Kelly, G., F. Rabier, J. Pailleux, and J. Thépaut, 1993: Observing system experiments made with the ECMWF system. Relevance to the development of some observing systems. Tech. Rep. 16, WMO/TD 594, 28 pp.

Lenschow, D., 1986: Aircraft measurements in the boundary layer. *Probing the Atmospheric Boundary Layer,* D. Lenschow, Ed., Amer. Meteor. Soc., 39–55.

Lorenc, A., R. Bell, T. Davies, and G. Shutts, 1988: Numerical forecast studies of the October 1987 storm over southern England. *Meteor. Mag.,* **117,** 118–130.

Petterssen, S., 1955: A general survey of factors influencing development at sea level. *J. Meteor.,* **12,** 36–42.

——, and S. Smebye, 1971: On the development of extratropical cyclones. *Quart. J. Roy. Meteor. Soc.,* **97,** 457–482.

Rabier, F., P. Courtier, and O. Talagrand, 1992: An application of adjoint models to sensitivity analysis. *Beitr. Phys. Atmos.,* **65,** 177–192.

——, E. Klinker, P. Courtier, and A. Hollingsworth, 1996: Sensitivity of forecast errors to initial conditions. *Quart. J. Roy. Meteor. Soc.,* **122,** 121–150.

Sutcliffe, R., 1947: A contribution to the problem of development. *Quart. J. Roy. Meteor. Soc.,* **73,** 370–383.

Talagrand, O., and P. Courtier, 1987: Variational assimilation of meteorological observations with the adjoint vorticity equation—Part 1. Theory. *Quart. J. Roy. Meteor. Soc.,* **113,** 1311–1328.

Warrenfeltz, L., and R. Elsberry, 1989: Superposition effects in rapid cyclogenesis—Linear model studies. *J. Atmos. Sci.,* **46,** 789–802.